



Giant Optical Activity and Second Harmonic Generation in 2D Hybrid Copper Halides

Zhihang Guo⁺, Junzi Li⁺, Changshun Wang, Rulin Liu, Jiechun Liang, Yang Gao, Jiaji Cheng, Wenjing Zhang, Xi Zhu,* Ruikun Pan,* and Tingchao He*

Abstract: Hybrid organic–inorganic metal halides have emerged as highly promising materials for a wide range of applications in optoelectronics. Incorporating chiral organic molecules into metal halides enables the extension of their unique optical and electronic properties to chiral optics. By using chiral (*R*)- or (*S*)-methylbenzylamine (*R/S*-MBA) as the organic component, we synthesized chiral hybrid copper halides, (*R/S*-MBA)₂CuCl₄, and investigated their optical activity. Thin films of this material showed a record anisotropic *g*-factor as high as approximately 0.06. We discuss the origin of the giant optical activity observed in (*R/S*-MBA)₂CuCl₄ by theoretical modeling based on density functional theory (DFT) and demonstrate highly efficient second harmonic generation (SHG) in these samples. Our study provides insight into the design of chiral materials by structural engineering, creating a new platform for chiral and nonlinear photonic device applications of the chiral hybrid copper halides.

Chirality, a ubiquitous phenomenon in nature, occurs in structures that lack S_n symmetry elements; thus, chiral structures cannot be superimposed on their mirror images.^[1] As a consequence of possessing non-centrosymmetric structures, chiral materials tend to exhibit unique optical properties, such as circular dichroism (CD) due to the difference in absorption of left- and right-hand circularly polarized (LCP and RCP) light and circularly polarized luminescence (CPL) due to the difference in LCP and RCP emission. The development and design of chiral materials for multidisciplinary applications in biometric detection and sensing,^[2] chiral bioimaging,^[3] and polarization-based optoelectronic devices have attracted immense interest.^[4]

Hybrid organic–inorganic metal halides, featuring structural versatility and unique photophysical properties, have recently emerged as promising semiconducting materials for high-performance optoelectronic applications.^[5] The variable lattice structure and molecular composition offer tremendous possibilities for tuning their optoelectronic properties. In particular, hybrid metal halides with organic sites allow for the introduction of chiral organic molecules, which further extends their applications in the field of chiral optoelectronics.^[6] Since Moon and co-workers first investigated the chiral optical properties of two-dimensional (2D) (*R/S*-MBA)₂PbI₄ (MBA = α -methylbenzylamine),^[7] chiral hybrid metal halides have prompted intensive research interest. Subsequently, great efforts have been devoted to synthesizing various chiral hybrid metal halides through changing the organic component, metal ion or halogen element, investigating their optical activity, and developing their diverse applications such as CPL sources,^[8] circularly polarized light detectors,^[9] and spintronics.^[10] For example, Li and co-authors developed 2D (*R/S*-MBA)₂PbI₄ and investigated their CPL and circularly polarized light detection.^[8b] Very recently, using one-dimensional (*R/S*-NEA)PbI₃ (NEA = 1-(1-naphthyl)ethylamine) with a highly anisotropic factor of 0.04, Ishii and Miyasaka fabricated a circularly polarized light detector, which achieved a polarization discrimination ratio as high as approximately 25.4.^[9a] Sargent and co-workers demonstrated a 3% spin-polarized photoluminescence of reduced-dimensional chiral perovskites even in the absence of an applied external magnetic field.^[10a] Due to their non-centrosymmetric structure, chiral hybrid metal halides can also be applied for second harmonic generation (SHG).^[11] For example, Xu and co-workers determined second-order nonlinear optical

[*] Z. Guo,^[†] J. Li,^[†] Prof. Y. Gao, Prof. T. He
Key Laboratory of Optoelectronic Devices and Systems of Ministry of Education and Guangdong Province, College of Physics and Optoelectronic Engineering, Shenzhen University
Shenzhen 518060 (China)
E-mail: tche@szu.edu.cn

Z. Guo,^[†] Prof. J. Cheng, Prof. R. Pan
Key Laboratory for the Green Preparation and Application of Functional Materials, Ministry of Education
School of Materials Science and Engineering, Hubei University
Wuhan 430062 (China)
E-mail: rkpan@hubu.edu.cn

J. Li,^[†] Prof. W. Zhang
SZU-NUS Collaborative Innovation Center for Optoelectronic Science and Technology, International Collaborative Laboratory of 2D Materials for Optoelectronics Science and Technology of Ministry of Education, College of Physics and Optoelectronic Engineering

Shenzhen University
Shenzhen 518060 (China)

Prof. C. Wang
State Key Laboratory of Advanced Optical Communication Systems and Networks, School of Physics and Astronomy
Shanghai Jiao Tong University
Shanghai 200240 (China)

R. Liu, J. Liang, Prof. X. Zhu
School of Science and Engineering
The Chinese University of Hong Kong
Shenzhen, Guangdong 518172 (China)
E-mail: zhuxi@cuhk.edu.cn

[†] These authors contributed equally to this work.

Supporting information and the ORCID identification number(s) of the author(s) of this article can be found under:
<https://doi.org/10.1002/anie.202015445>.

(NLO) coefficient of $(R/S\text{-MPEA})_{1.5}\text{PbBr}_{3.5}(\text{DMSO})_{0.5}$ (MPEA = β -methylphenethylamine) as approximately 0.68 pm V^{-1} at 850 nm .^[12] Very recently, a series of chiral metal halides were manufactured by Heine and co-workers,^[13] and the SHG signals were 5–45 times smaller than the quartz reference.

Although great progress in the investigation on the optical activity of hybrid metal halides has been made, there is still extensive room for improving their optical activity. Obviously, advancements in exploring new chiral hybrid metal halides are in high demand. Towards this end, the design, synthesis, and characterization of hybrid metal halides with large optical activity are urgently required for the realization of relevant applications.

Herein, we report the synthesis of thin films of the chiral 2D hybrid metal halides, (R) - or (S) -methylbenzylammonium copper chloride $((R/S\text{-MBA})_2\text{CuCl}_4)$. The as-prepared films exhibit strong mirrored CD signals with a giant anisotropic g -factor of approximately 0.06, which is even greater than the record value (ca. 0.04) recently reported for chiral $(R/S\text{-NEA})\text{PbI}_3$.^[9a] We discuss the origin of giant optical activity in these samples through theoretical modeling based on density functional theory (DFT). Significantly, the chiral $(R/S\text{-MBA})_2\text{CuCl}_4$ films exhibited high second-order NLO coefficients that are estimated to be approximately 50 times larger than the Y -cut quartz reference.

$(R/S\text{-MBA})_2\text{CuCl}_4$ thin films were prepared by a spin-coating approach using chiral R - or S -MBA as the organic component (see details in the Supporting Information). The lattice structures of $(R\text{-MBA})_2\text{CuCl}_4$ and $(S\text{-MBA})_2\text{CuCl}_4$ are characteristic of 2D layered materials (Figure 1 a), where each central Cu atom coordinates with four Cl atoms to form $[\text{CuCl}_4]^{2-}$ tetrahedra that are sandwiched between two layers

of chiral R - or S -MBA molecules. $(R/S\text{-MBA})_2\text{CuCl}_4$ crystallizes in the polar and chiral C_2 space group (C_2 point group), assigned to the monoclinic crystal system.^[14] X-ray diffraction (XRD) patterns of both $(R/S\text{-MBA})_2\text{CuCl}_4$ exhibit sharp diffraction peaks that can be assigned to the $(0\ 0\ l)$ planes (Figure 1 b), suggesting that the orientation of the $[\text{CuCl}_4]^{2-}$ tetrahedral inorganic layers is highly parallel to the substrate plane. The narrow full width at half maximum of the XRD patterns further indicates the excellent crystallinity of the as-prepared films. Atomic force microscopy (AFM) measurements were used to determine the morphology and thickness of the two chiral films (Supporting Information, Figure S1). The low roughness with an R_a (average surface roughness) of approximately 6 nm indicated the uniform morphology of the solid films.

UV–vis absorption and CD spectra of the ammonium halide salts and $(R/S\text{-MBA})_2\text{CuCl}_4$ films are shown in Figure 1 c,d, respectively. The ammonium halide salts R - or S -MBACL (chemical structures shown in the inset of Figure 1 c) show mirrored CD signals below 280 nm, with a peak at 268 nm. However, much stronger CD signals were observed in the $(R/S\text{-MBA})_2\text{CuCl}_4$ films from the ultraviolet to visible regions, indicating that the chirality could not be entirely ascribed to the pure ammonium halide salts. $(R/S\text{-MBA})_2\text{CuCl}_4$ exhibited mirrored CD signals peaking at 378, 266, and 226 nm, which are consistent with their absorption bands, as a result of the Cotton effect.^[15] In addition, the peak at 378 nm corresponds to the characteristic ligand-to-metal charge transfer (LMCT) transition band of $[\text{CuCl}_4]^{2-}$,^[16] as a consequence of charge transfer from fully occupied chloride ion localized orbitals or $\sigma_{\text{Cu-Cl}}$ and $\pi_{\text{Cu-Cl}}$ orbitals to copper ion semioccupied d_{xy} orbital.^[17] These results demonstrate that the chirality of the organic component was successfully

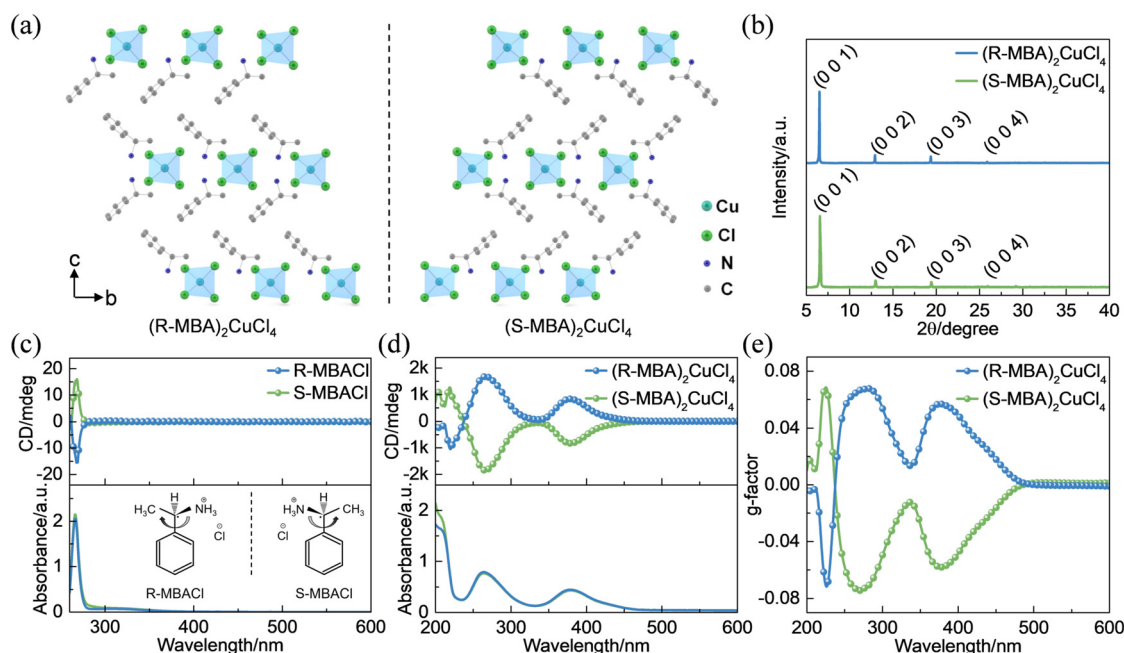


Figure 1. a) Lattice structure of $(R/S\text{-MBA})_2\text{CuCl}_4$. H atoms are omitted for clarity. b) XRD patterns of $(R/S\text{-MBA})_2\text{CuCl}_4$ films. c) CD and absorption spectra of the ammonium halide salts dissolved in dimethylformamide (10 mg mL^{-1}). Inset shows the chemical structures of R/S -MBACL. d) CD and absorption spectra of $(R/S\text{-MBA})_2\text{CuCl}_4$ films. e) Corresponding g -factor spectra.

transferred to the internal structural framework. Notably, the anisotropic g-factor, which is defined as $|g_{\text{CD-}} - g_{\text{CD+}}|/2$,^[18] was calculated to be approximately 0.06 at the LMCT band of $[\text{CuCl}_4]^{2-}$ (Figure 1 e), which is one order of magnitude larger than that of the chiral $(\text{R}/\text{S-MBA})_2\text{PbI}_4$ hybrid lead halides (ca. 0.006),^[7] and is even larger than the record value of 0.04 recently reported for the chiral one-dimensional $(\text{R}/\text{S-NEA})\text{PbI}_3$.^[9a] Additionally, the CD spectra of $(\text{R}/\text{S-MBA})_2\text{CuCl}_4$ did not change significantly after being stored under ambient conditions for one month, demonstrating the excellent long-term stability of the as-prepared films (Supporting Information, Figure S2).

In order to reveal the origin of giant g-factors in chiral $(\text{R}/\text{S-MBA})_2\text{CuCl}_4$, theoretical calculation on their optical activity was performed. The CD intensity can be calculated by Equation (1):^[19]

$$\text{CD} = w^{(L)} - w^{(R)} \quad (1)$$

where w denotes the transition probability density per unit time, L and R refer to LCP and RCP light, respectively. The transition was shown to be proportional to the probability of the transition,^[20] that is, the joint density of states (JDOS). As the JDOS of transition ($J(\hbar\omega)$) with energy $\hbar\omega$ can be expressed as^[21]

$$J(\hbar\omega) = \int_{-\infty}^{+\infty} N_v(E)N_c(E + \hbar\omega)dE \quad (2)$$

where $N_{v,c}$ refers to the JDOS on the valence and conduction band. Thus, the g-factor from the JDOS of a given material can be estimated.

In order to unveil the mechanism that causes much larger optical activity in $(\text{R}/\text{S-MBA})_2\text{CuCl}_4$ compared with $(\text{R}/\text{S-MBA})_2\text{PbI}_4$, their density of states was calculated by GW approximation. The self-consistent PWSCF is used, which can well establish LDA and GGA functionals with spin-polarization.^[22] As shown in Figure 2, the arrows indicate the transitions from the initial to final states. Different from regular DFT calculation, the GW method includes DFT and focuses on the quasiparticle situation, and the screening effects contribute more to the final result. In addition, the GW method can generate a wave function as a precalculation. It is noteworthy that the band gap value calculated by GW method is always larger than the experimentally measured one. The orbital distribution relevant to the chiral excitation was plotted (insets in Figure 2). Importantly, it was found that the orbitals were mainly distributed around the Cu/Pb atoms. This means that the JDOS for the chiral transition could be altered by the metal atoms. Compared with $(\text{R}/\text{S-MBA})_2\text{PbI}_4$, $(\text{R}/\text{S-MBA})_2\text{CuCl}_4$ possesses a higher JDOS, thus accounting for the enhanced g-factors by one order of magnitude in the latter. Actually, Kotov, Moon, and co-workers also investigated the effect of chemical-composition modification on the optical activity of $(\text{R}/\text{S-MBA})_2\text{PbI}_{4(1-x)}\text{Br}_{4x}$, whose g-factors can vary by one order of magnitude through the change of mixing ratio of bromide and iodide anions.^[23] However, the g-factors of $(\text{R}/\text{S-MBA})_2\text{PbI}_{4(1-x)}\text{Br}_{4x}$ were still an order of magnitude smaller

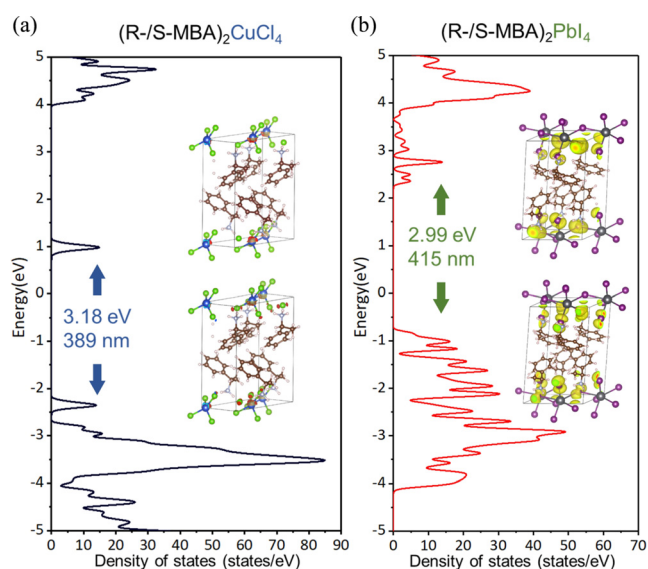


Figure 2. Density of states of a) $(\text{R}/\text{S-MBA})_2\text{CuCl}_4$ and b) $(\text{R}/\text{S-MBA})_2\text{PbI}_4$ according GW approximation calculation, and spatial distribution of the relevant orbitals. The arrows point to the initial and final states of the transitions. By multiplying the respective states shown in the figure, it can be observed that the JDOS of the copper-containing material is larger than that of the lead-containing material, thus accounting for the higher CD intensity observed in the former.

than $(\text{R}/\text{S-MBA})_2\text{CuCl}_4$, as a consequence of larger JDOS in the latter.

According to Fukui's method,^[24] the optical selectivity of circularly polarized light versus the band gap of the chiral $(\text{R}/\text{S-MBA})_2\text{CuCl}_4$ films was also calculated (Supporting Information, Figure S3), which can serve as a reference to identify the source of chirality. As a result of the optical activity of the hybrid copper halides, inverse optical selectivity to circularly polarized light was observed, with peaks at 2.96 and 3.18 eV for $(\text{R-MBA})_2\text{CuCl}_4$, and 2.93 and 3.17 eV for $(\text{S-MBA})_2\text{CuCl}_4$, respectively; this was in agreement with their measured absorption peak positions in the visible region. Importantly, our calculations indicated that the orbitals of the chiral carbons could not be coupled with those of copper or chlorine due to the long $\text{N-H}\cdots\text{Cl}$ and $\text{C-H}\cdots\pi$ hydrogen bonding. From the perspective of quantum theory, the chirality of the hybrid copper halides was a consequence of their chiral crystal structure (C_2 space group), which can be described as^[25]

$$\text{CD} \propto \mathbf{R} = \text{Im}\{\boldsymbol{\mu}\mathbf{m}\} \quad (3)$$

where \mathbf{R} is the theoretical rotational strength, Im is the imaginary part of the parameter, $\boldsymbol{\mu}$ is the electric dipole transition moment for the transition from the final to the initial state, and \mathbf{m} is the magnetic dipole transition for the reverse transition. The condition for the occurrence of chirality is that the electric and magnetic dipole moment operators must be converted into the same irreducible representation. Under such circumstances, both $(\text{R}/\text{S-MBA})_2\text{CuCl}_4$ crystallize in the C_2 point group, which makes

μ and m non-zero and induces optical chirality (Supporting Information, Table S1).

Furthermore, the SHG signals of the (R-MBA)₂CuCl₄ film were investigated to elucidate the feasibility in nonlinear optics. SHG measurements were carried out using a combined polarized light optical microscope in reflection geometry using perpendicular incident excitation (Supporting Information, Figure S4). The wavelength-dependent SHG spectra of the (R-MBA)₂CuCl₄ film was investigated at different excitation wavelengths with the same excitation power and strong SHG signals were observed in the chiral film with excitation wavelengths in the broad wavelength range of 780–920 nm (Figure 3a). Analysis of the pumping fluence-dependent SHG intensities under 800 nm excitation (inset in Figure 3a) revealed square relationship that confirmed the two-photon nature of this second-order NLO response. Additionally, the nonlinear efficiency of the (R-MBA)₂CuCl₄ film was evaluated by comparing the SHG signals with that of Y-cut quartz reference. The SHG signals of the (R-MBA)₂CuCl₄ and Y-cut quartz films were measured under the same conditions (including the incident laser power intensity). The second-order NLO coefficient of the chiral film is determined by using Y-cut quartz as a reference, and is given by^[26]

$$\frac{d_{\text{eff}}^s}{d_{\text{eff}}^r} \approx \sqrt{\frac{I_{2\omega}^s I_{\omega}^r L^r n_{\omega}^s}{I_{2\omega}^r I_{\omega}^s L^s n_{\omega}^r}} \sqrt{\frac{n_{2\omega}^s}{n_{2\omega}^r}} \quad (4)$$

where I_{ω} is the pump intensity, d_{eff} is the effective second-order NLO coefficients (the superscripts “s” and “r” refer to the hybrid copper halide film and Y-cut quartz, respectively; $d_{\text{eff}}^r = 0.6 \text{ pm V}^{-1}$,^[27] L is the effective thickness, and n_{ω} and $n_{2\omega}$ are the refractive indices at the frequency ω and 2ω , respectively. We used laser pumping under the same conditions (20 mW, 800 nm) and the SHG signals were detected at 400 nm for both films. The refractive indices of the Y-cut quartz at 800 and 400 nm are 1.54 and 1.56,^[28] respectively, while relevant values for the chiral film are 1.55 and 2.8 at 800 and 400 nm, respectively. Using the Y-cut quartz as a reference, d_{eff} of the chiral (R-MBA)₂CuCl₄ film was determined to be approximately 28.75 pm V^{-1} with the optimized linearly

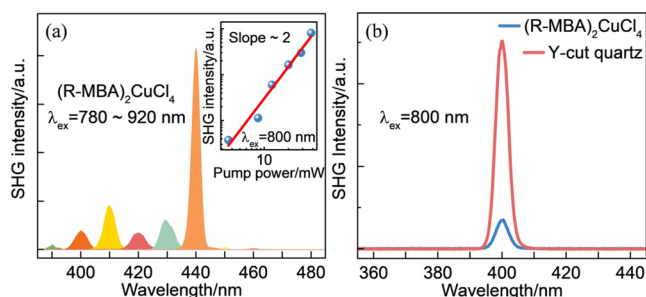


Figure 3. a) Wavelength-dependent SHG signals of (R-MBA)₂CuCl₄. Inset: Plot of SHG intensity versus pump power; the slope of approximately 2 confirms the SHG mechanism. The laser damage threshold was approximately 3.31 GW cm^{-2} , as determined under 800 nm excitation (100 fs, 80 MHz). b) Comparison of the SHG intensities of (R-MBA)₂CuCl₄ with a thickness of approximately $0.6 \mu\text{m}$ and Y-cut quartz with a thickness of $50 \mu\text{m}$.

polarized pump light at 800 nm. Because the accurate determination of their second-order NLO coefficients depends on the actual experimental parameters and the reabsorption effect must be considered, the d_{eff} value of the chiral (R-MBA)₂CuCl₄ film is an estimation on the order of magnitude. Importantly, this value is several orders of magnitude larger than the previously reported chiral (R-/S-MPEA)_{1.5}PbBr_{3.5}(DMSO)_{0.5} (0.68 pm V^{-1} , 850 nm),^[12] and comparable to that for CH₃C(NH₂)₂GeI₃ (57.2 pm V^{-1} , 1064 nm) single crystals.^[29]

In summary, we synthesized chiral 2D hybrid metal halides, that is, (R-/S-MBA)₂CuCl₄, and they exhibit a record anisotropic g-factor of approximately 0.06 at the LMCT band of [CuCl₄]²⁻. Theoretical calculations confirm that the larger optical activity of (R-/S-MBA)₂CuCl₄ compared with other chiral hybrid metal halides is induced by the higher JDOS in the former. In addition, it is also theoretically proven that the chirality in the hybrid copper halides is induced by the chiral crystal structure (chiral space group). Impressively, the second-order NLO coefficients of the chiral (R-/S-MBA)₂CuCl₄ films are about 50 times larger than that of the Y-cut quartz reference at 800 nm. This work demonstrates the tremendous potential of the chiral hybrid copper halides for chiral and nonlinear photonic applications.

Acknowledgements

We acknowledge financial support by the Guangdong Basic and Applied Basic Research Foundation (2019A1515012094), the Project of Department of Education of Guangdong Province (2018KTSCX19), the Science and Technology Planning Project of Shenzhen Municipality (JCYJ20190808121211510), the National Natural Science Foundation of China (92050116, 21805234, 22075240), the Shenzhen Institute of Artificial Intelligence and Robotics for Society (AIRS; 2019-INT018,2020-IND002) and the Guangdong Introducing Innovative and Entrepreneurial Teams (2019ZT08L101).

Conflict of interest

The authors declare no conflict of interest.

Keywords: chirality · circular dichroism · hybrid copper halides · nonlinear optics · second harmonic generation

- [1] J. A. Schellman, *J. Chem. Phys.* **1966**, *44*, 55–63.
- [2] a) Y. Zhao, C. Xu, *Adv. Mater.* **2020**, *32*, 1907880; b) C. Hao, A. Qu, L. Xu, M. Sun, H. Zhang, C. Xu, H. Kuang, *J. Am. Chem. Soc.* **2019**, *141*, 1091–1099.
- [3] a) F. Gao, M. Sun, W. Ma, X. Wu, L. Liu, H. Kuang, C. Xu, *Adv. Mater.* **2017**, *29*, 1606864; b) M. Sun, A. Qu, C. Hao, X. Wu, L. Xu, C. Xu, H. Kuang, *Adv. Mater.* **2018**, *30*, 1804241.
- [4] Z.-G. Wu, H.-B. Han, Z.-P. Yan, X.-F. Luo, Y. Wang, Y.-X. Zheng, J.-L. Zuo, Y. Pan, *Adv. Mater.* **2019**, *31*, 1900524.
- [5] L. Gao, L. N. Quan, F. P. García de Arquer, Y. Zhao, R. Munir, A. Proppe, R. Quintero-Bermudez, C. Zou, Z. Yang,

- M. I. Saidaminov, O. Voznyy, S. Kinge, Z. Lu, S. O. Kelley, A. Amassian, J. Tang, E. H. Sargent, *Nat. Photonics* **2020**, *14*, 227–233; b) Y.-H. Lin, N. Sakai, P. Da, J. Wu, H. C. Sansom, A. J. Ramadan, S. Mahesh, J. Liu, R. D. J. Oliver, J. Lim, L. Aspirtarte, K. Sharma, P. K. Madhu, A. B. Morales-Vilches, P. K. Nayak, S. Bai, F. Gao, C. R. M. Grovenor, M. B. Johnston, J. G. Labram, J. R. Durrant, J. M. Ball, B. Wenger, B. Stannowski, H. J. Snaith, *Science* **2020**, *369*, 96–102; c) S.-X. Li, Y.-S. Xu, C.-L. Li, Q. Guo, G. Wang, H. Xia, H.-H. Fang, L. Shen, H.-B. Sun, *Adv. Mater.* **2020**, *32*, 2001998; d) C. Qin, A. S. D. Sandanayaka, C. Zhao, T. Matsushima, D. Zhang, T. Fujihara, C. Adachi, *Nature* **2020**, 585, 53–57.
- [6] G. Long, R. Sabatini, M. I. Saidaminov, G. Lakhwani, A. Rasmita, X. Liu, E. H. Sargent, W. Gao, *Nat. Rev. Mater.* **2020**, *5*, 423–439.
- [7] J. Ahn, E. Lee, J. Tan, W. Yang, B. Kim, J. Moon, *Mater. Horiz.* **2017**, *4*, 851–856.
- [8] a) J. Ma, C. Fang, C. Chen, L. Jin, J. Wang, S. Wang, J. Tang, D. Li, *ACS Nano* **2019**, *13*, 3659–3665; b) J. Wang, C. Fang, J. Ma, S. Wang, L. Jin, W. Li, D. Li, *ACS Nano* **2019**, *13*, 9473–9481; c) D. Di Nuzzo, L. Cui, J. L. Greenfield, B. Zhao, R. H. Friend, S. C. J. Meskers, *ACS Nano* **2020**, *14*, 7610–7616.
- [9] a) A. Ishii, T. Miyasaka, *Sci. Adv.* **2020**, *6*, eabd3274; b) C. Chen, L. Gao, W. Gao, C. Ge, X. Du, Z. Li, Y. Yang, G. Niu, J. Tang, *Nat. Commun.* **2019**, *10*, 1927; c) L. Wang, Y. Xue, M. Cui, Y. Huang, H. Xu, C. Qin, J. Yang, H. Dai, M. Yuan, *Angew. Chem. Int. Ed.* **2020**, *59*, 6442–6450; *Angew. Chem.* **2020**, *132*, 6504–6512.
- [10] a) G. Long, C. Jiang, R. Sabatini, Z. Yang, M. Wei, L. N. Quan, Q. Liang, A. Rasmita, M. Askerka, G. Walters, X. Gong, J. Xing, X. Wen, R. Quintero-Bermudez, H. Yuan, G. Xing, X. R. Wang, D. Song, O. Voznyy, M. Zhang, S. Hoogland, W. Gao, Q. Xiong, E. H. Sargent, *Nat. Photonics* **2018**, *12*, 528–533; b) H. Lu, J. Wang, C. Xiao, X. Pan, X. Chen, R. Brunecky, J. J. Berry, K. Zhu, M. C. Beard, Z. V. Vardeny, *Sci. Adv.* **2019**, *5*, eaay0571.
- [11] R.-G. Xiong, S.-Q. Lu, Z.-X. Zhang, H. Cheng, P.-F. Li, W.-Q. Liao, *Angew. Chem. Int. Ed.* **2020**, *59*, 9574–9578; *Angew. Chem.* **2020**, *132*, 9661–9665.
- [12] C. Yuan, X. Li, S. Semin, Y. Feng, T. Rasing, J. Xu, *Nano Lett.* **2018**, *18*, 5411–5417.
- [13] N. Dehnhardt, M. Axt, J. Zimmermann, M. Yang, G. Mette, J. Heine, *Chem. Mater.* **2020**, *32*, 4801–4807.
- [14] A. M. Ben Salah, N. Sayari, H. Naili, A. J. Norquist, *RSC Adv.* **2016**, *6*, 59055–59065.
- [15] J. A. Schellman, P. Oriol, *J. Chem. Phys.* **1962**, *37*, 2114–2124.
- [16] a) A. S. Mereshchenko, O. S. Myasnikova, P. K. Olshin, S. M. Matveev, M. S. Panov, V. A. Kochemirovsky, M. Y. Skripkin, A. N. Tarnovsky, *J. Phys. Chem. B* **2018**, *122*, 10558–10571; b) D. W. Smith, *Coord. Chem. Rev.* **1976**, *21*, 93–158; c) B. J. Hathaway, *J. Chem. Soc. Dalton Trans.* **1972**, 1196–1199; d) H.-B. Yi, F.-F. Xia, Q. Zhou, D. Zeng, *J. Phys. Chem. A* **2011**, *115*, 4416–4426.
- [17] J. Ferguson, *J. Chem. Phys.* **1964**, *40*, 3406–3410.
- [18] J. Hao, Y. Li, J. Miao, R. Liu, J. Li, H. Liu, Q. Wang, H. Liu, M.-H. Delville, T. He, K. Wang, X. Zhu, J. Cheng, *ACS Nano* **2020**, *14*, 10346–10358.
- [19] A. Rodger, *Encyclopedia of Biophysics* (Ed.: G. C. K. Roberts), Springer Berlin Heidelberg, Berlin, **2013**, pp. 311–313.
- [20] M. Wakabayashi, S. Yokojima, T. Fukaminato, K.-i. Shiino, M. Irie, S. Nakamura, *J. Phys. Chem. A* **2014**, *118*, 5046–5057.
- [21] S. K. O’Leary, *J. Appl. Phys.* **2004**, *96*, 3680–3686.
- [22] P. Giannozzi, S. Baroni, N. Bonini, M. Calandra, R. Car, C. Cavazzoni, D. Ceresoli, G. L. Chiarotti, M. Cococcioni, I. Dabo, A. Dal Corso, S. de Gironcoli, S. Fabris, G. Fratesi, R. Gebauer, U. Gerstmann, C. Gougousis, A. Kokalj, M. Lazzeri, L. Martin-Samos, N. Marzari, F. Mauri, R. Mazzarello, S. Paolini, A. Pasquarello, L. Paulatto, C. Sbraccia, S. Scandolo, G. Sclauzero, A. P. Seitsonen, A. Smogunov, P. Umari, R. M. Wentzcovitch, *J. Phys. Condens. Matter* **2009**, *21*, 395502.
- [23] J. Ahn, S. Ma, J.-Y. Kim, J. Kyhm, W. Yang, J. A. Lim, N. A. Kotov, J. Moon, *J. Am. Chem. Soc.* **2020**, *142*, 4206–4212.
- [24] T. Fukui, Y. Hatsugai, H. Suzuki, *J. Phys. Soc. Jpn.* **2005**, *74*, 1674–1677.
- [25] M. K. Jana, R. Song, H. Liu, D. R. Khanal, S. M. Janke, R. Zhao, C. Liu, Z. Valy Vardeny, V. Blum, D. B. Mitzi, *Nat. Commun.* **2020**, *11*, 4699.
- [26] T. A. Theodossiou, C. Thrasivoulou, C. Ekwobi, D. L. Becker, *Biophys. J.* **2006**, *91*, 4665–4677.
- [27] A. Hermans, “Low-Temperature Processed Thin Films of Second-Order Nonlinear Optical Materials for Silicon Nitride Photonic Integrated Circuits”, Ghent University, Faculty of Engineering and Architecture, **2019**, p. 4–19.
- [28] G. Ghosh, *Opt. Commun.* **1999**, *163*, 95–102.
- [29] C. C. Stoumpos, L. Frazer, D. J. Clark, Y. S. Kim, S. H. Rhim, A. J. Freeman, J. B. Ketterson, J. I. Jang, M. G. Kanatzidis, *J. Am. Chem. Soc.* **2015**, *137*, 6804–6819.

Manuscript received: November 19, 2020

Accepted manuscript online: January 22, 2021

Version of record online: March 1, 2021